RESEARCH ARTICLE SUMMARY

CARBON CYCLE

The Orbiting Carbon Observatory-2 early science investigations of regional carbon dioxide fluxes

A. Eldering,* P. O. Wennberg, D. Crisp, D. S. Schimel, M. R. Gunson, A. Chatterjee, J. Liu, F. M. Schwandner, Y. Sun, C. W. O'Dell, C. Frankenberg, T. Taylor, B. Fisher, G. B. Osterman, D. Wunch, J. Hakkarainen, J. Tamminen, B. Weir

INTRODUCTION: Earth's carbon cycle involves large fluxes of carbon dioxide (CO_2) between the atmosphere, land biosphere, and oceans. Over the past several decades, net loss of CO_2 from the atmosphere to the land and oceans has varied considerably from year to year, equaling 20 to 80% of CO_2 emissions from fossil fuel combustion and land use change. On average, the uptake is about 50%. The imbalance between CO_2 emissions and removal is seen in increasing atmospheric CO_2 concentrations. In recent years, an increase of 2 to 3 parts per million (ppm) per year in the atmospheric mole fraction, which is currently about 400 ppm, has been observed.

Almost a quarter of the CO_2 emitted by human activities is being absorbed by the ocean, and another quarter is absorbed by processes on land. The identity and location of the terrestrial sinks are poorly understood. This absorption has been attributed by some to tropical or Eurasian temperate forests, whereas others argue that these regions may be net sources of CO_2. The efficiency of these land sinks appears to vary dramatically from year to year. Because the identity, location, and processes controlling these natural sinks are not well constrained, substantial additional uncertainty is added to projections of future CO_2 levels.

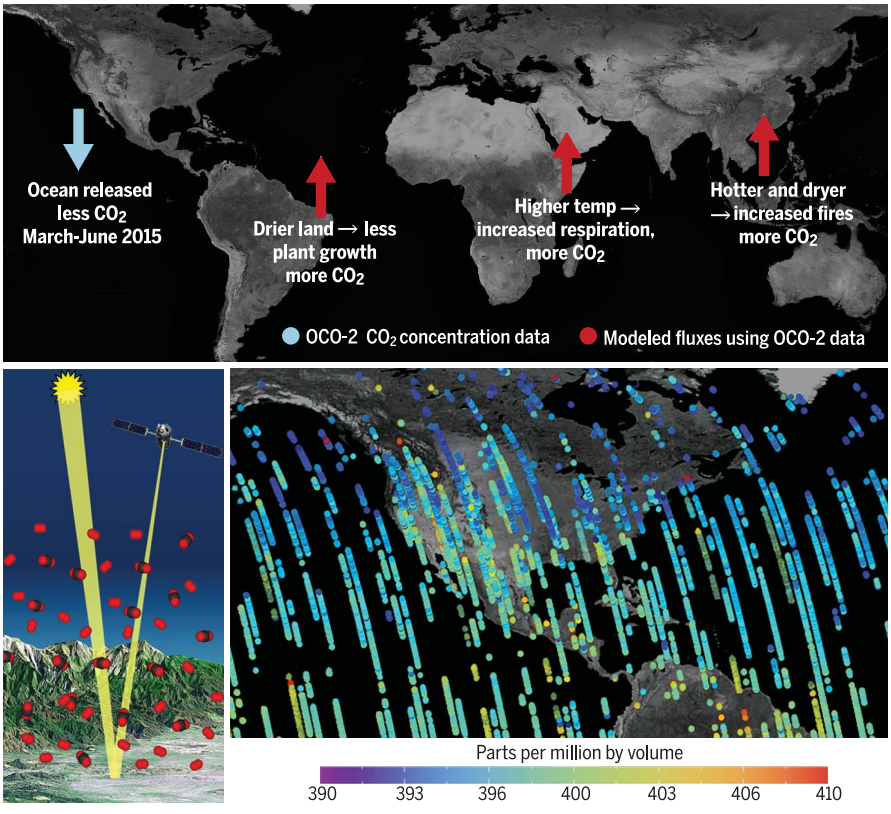

El Niño impact on carbon flux in 2015 relative to 2011, detected from Greenhouse Gases Observing Satellite (GOSAT) and OCO-2 data. OCO-2 uses reflected sunlight to derive X_{CO_2} and SIF. This shows OCO-2 X_{CO_2} data over North America from 12 August 2015 to 26 August 2015.

RATIONALE: The NASA satellite, the Orbiting Carbon Observatory-2 (OCO-2), which was launched on 2 July 2014, is designed to collect global measurements with sufficient precision, coverage, and resolution to aid in resolving sources and sinks of CO_2 on regional scales. Since 6 September 2014, the OCO-2 mission has been producing about 2 million estimates of the column-averaged CO_2 dry-air mole fraction (X_{CO_2}) each month after quality screening, with spatial resolution of <3 km^2 per sounding. Solar-induced chlorophyll fluorescence (SIF), a small amount of light emitted during photosynthesis, is detected in remote sensing measurements of radiance within solar Fraunhofer lines and is another data product from OCO-2.

ON OUR WEBSITE

Read the full article at http://dx.doi.org/10.1126/science.aam5745

RESULTS: The measurements from OCO-2 provide a global view of the seasonal cycles and spatial patterns of atmospheric CO_2, with the anticipated year-over-year growth rate. The buildup of CO_2 in the Northern Hemisphere during winter and its rapid decrease in concentration as spring arrives (and the SIF increases) is seen in unprecedented detail. The enhanced CO_2 in urban areas relative to nearby background areas is observed with a single overpass of OCO-2. Increases in CO_2 due to the biomass burning in Africa are also clearly observed. The dense, global, X_{CO_2} and SIF data sets from OCO-2 are combined with other remote sensing data sets and used to disentangle the processes driving the carbon cycle on regional scales during the recent 2015–2016 El Niño event. This analysis shows more carbon release in 2015 relative to 2011 over Africa, South America, and Southeast Asia. Now, the fundamental driver for the change in carbon release can be assessed continent by continent, rather than treating the tropics as a single, integrated region. Small changes in X_{CO_2} were also observed early in the El Niño over the equatorial eastern Pacific, due to less upwelling of cold, carbon-rich water than is typical.

CONCLUSION: NASA's OCO-2 mission is collecting a dense, global set of high-spectral resolution measurements that are used to estimate X_{CO_2} and SIF. The OCO-2 mission data set can now be used to assess regional-scale sources and sinks of CO_2 around the globe. The papers in this collection present early scientific findings from this new data set. ■

The list of author affiliations is available in the full article online.
*Corresponding author. Email: annmarie.eldering@jpl.nasa.gov
Cite this article as A. Eldering *et al.*, *Science* **358**, eaam5745 (2017). DOI: 10.1126/science.aam5745

RESEARCH ARTICLE

CARBON CYCLE

The Orbiting Carbon Observatory-2 early science investigations of regional carbon dioxide fluxes

A. Eldering,[1]* P. O. Wennberg,[2,3] D. Crisp,[1] D. S. Schimel,[1] M. R. Gunson,[1] A. Chatterjee,[4,5] J. Liu,[1] F. M. Schwandner,[1] Y. Sun,[1] C. W. O'Dell,[6] C. Frankenberg,[2] T. Taylor,[6] B. Fisher,[1] G. B. Osterman,[1] D. Wunch,[2]† J. Hakkarainen,[7] J. Tamminen,[7] B. Weir[4,5]

NASA's Orbiting Carbon Observatory-2 (OCO-2) mission was motivated by the need to diagnose how the increasing concentration of atmospheric carbon dioxide (CO_2) is altering the productivity of the biosphere and the uptake of CO_2 by the oceans. Launched on 2 July 2014, OCO-2 provides retrievals of the column-averaged CO_2 dry-air mole fraction (X_{CO_2}) as well as the fluorescence from chlorophyll in terrestrial plants. The seasonal pattern of uptake by the terrestrial biosphere is recorded in fluorescence and the drawdown of X_{CO_2} during summer. Launched just before one of the most intense El Niños of the past century, OCO-2 measurements of X_{CO_2} and fluorescence record the impact of the large change in ocean temperature and rainfall on uptake and release of CO_2 by the oceans and biosphere.

Large fluxes of carbon dioxide (CO_2) between the atmosphere, land biosphere, and oceans (*1*) occur within Earth's carbon cycle. The exchange varies seasonally, with net carbon uptake into the terrestrial biosphere during the growing season, especially in the Northern Hemisphere. In the fall and winter, photosynthesis declines in the mid- and high latitudes, and plant respiration exceeds photosynthesis, returning CO_2 to the atmosphere. Continuing emissions of CO_2 from fossil fuels adds carbon to the atmosphere, mostly in the Northern Hemisphere (*2*). The uptake of CO_2 from the atmosphere into the land and oceans constitutes between 20 and 80% of CO_2 emissions from fossil fuel and land use change (*3*, *4*) and is ~50% on average. The balance—that is, the fraction of anthropogenic carbon release not reabsorbed by the Earth System—is referred to as the "airborne fraction." It is manifest in the rising burden of atmospheric CO_2, whose concentration is increasing 0.50 to 0.75% each year [2 to 3 parts per million (ppm) per year increase in the atmospheric mole fraction] (*5*).

Subtle geographic and temporal variations in atmospheric concentrations of CO_2, of fractions of a ppm to several ppm of the ambient ~400 ppm background, reflect the underlying uptake and release of carbon. These variations provide clues to the underlying mechanisms that drive differences in the airborne fraction. Measurements of the increasing inventory of carbon in seawater indicate that almost a quarter of the CO_2 emitted by human activities is being absorbed by the ocean (*6*), where it contributes to ocean acidification. Mass balance demands that another quarter of the CO_2 emitted by human activities must be absorbed by processes on land. The identity and location of these sinks are less well understood. Some studies have attributed this absorption to tropical (*7*) or Eurasian temperate (*8*) forests, whereas others indicate that these areas are just as likely to be net sources as net sinks of CO_2 (*9*). The efficiency of these natural land and ocean sinks also appears to vary dramatically from year to year (*3*). Because the identity, location, and processes controlling these natural sinks are not well constrained, it is not clear how they will respond in the future (*7*). Understanding these mechanisms and their dependence on climate and atmospheric CO_2 levels is central to understanding how the carbon cycle may amplify or mitigate future climate change (*3*, *7*, *10*–*13*).

Measuring CO_2 from space with OCO-2

The international network of ground-based in situ greenhouse gas measurement stations provides a long-term and precise (~0.07 ppm) record of the atmospheric CO_2 concentration at ~147 locations across the globe (*14*, *15*). Few measurements are obtained in tropical regions, in urban settings, or in Asia. The NASA satellite, the Orbiting Carbon Observatory-2 (OCO-2), which was launched from Vandenberg Air Force Base in California on 2 July 2014, is designed to collect global measurements with sufficient precision, coverage, and resolution to aid in resolving sources and sinks on regional scales. After completing a series of spacecraft check-out activities and orbit-raising maneuvers, on 3 August 2014, it joined the front of the Afternoon Constellation (A-Train) (*16*), which consists of six satellites orbiting at an altitude of 705 km. In this 98.8-min orbit, OCO-2 samples at a local time of about 1:30 p.m., and it has a set of 233 orbit paths that repeat in 16-day cycles. The OCO-2 sampling strategy repeats in 32-day cycles. Since 6 September 2014, the OCO-2 instrument has been routinely returning almost 1 million soundings each day over the sunlit hemisphere. This measurement concept was developed in the late 1990s, but this type of data has only been collected since 2014. The OCO-2 mission is a replacement for the original OCO instrument and spacecraft that were lost in a failed launch in February 2009; only small modifications to replace obsolete parts and to adapt to a different launch vehicle were required.

The OCO-2 spectrometers collect eight spatially resolved radiance spectra of reflected sunlight in three narrow wavelength bands three times per second, with resolving power ($\Delta\lambda/\lambda$) of ~17,000 (Fig. 1) (*17*–*19*). The oxygen A-band (centered at ~765 nm) provides a sensitive measure of the atmospheric path length and is thus an accurate indicator of clouds and surface elevation. The radiance at two distinct CO_2 absorption bands (1.61 and 2.06 μm) provides sensitivity to CO_2. The column-averaged atmospheric CO_2 dry-air mole fraction (X_{CO_2}), or the total column of carbon dioxide normalized by the column of dry air, is derived from these spectra using a physics-based retrieval method (*20*–*22*). The sensitivity of the measurement is fairly uniform throughout the troposphere and lower stratosphere and varies with solar geometry and surface (*23*). Details of the instrument calibration and observatory operation are reported in Crisp *et al.* (*19*), and the data processing strategy is described by Eldering *et al.* (*24*).

A set of eight measurements are made along a narrow ground track as the spacecraft travels about 2.25 km along its orbit track, providing spatial resolution of <3 km^2 per sounding. X_{CO_2} is retrieved only when there is sufficient light (solar zenith angles less than 85°) and when there are no optically thick clouds (*25*). OCO-2 returns roughly 2 million X_{CO_2} estimates each month that pass quality screening (Fig. 2), for a yield of about 6% of the total soundings.

Systematic biases in the OCO-2 X_{CO_2} estimates must be minimized to accurately resolve the small spatial and temporal variations in this quantity. The bias correction, designed to address known systematic errors, takes advantage of the high density of soundings gathered over regions with minimal variability in X_{CO_2} (such as contiguous data collected in small areas and over the Southern Hemisphere oceans) (*26*, *27*). To relate the OCO-2 X_{CO_2} estimates to the standard CO_2 scale set by the international CO_2 in situ network, we

[1]Jet Propulsion Laboratory, California Institute of Technology, Pasadena, CA, USA. [2]Division of Geology and Planetary Sciences, California Institute of Technology, Pasadena, CA, USA. [3]Division of Engineering and Applied Science, California Institute of Technology, Pasadena, CA, USA. [4]Universities Space Research Association, Columbia, MD, USA. [5]NASA Global Modeling and Assimilation Office, Greenbelt, MD, USA. [6]Cooperative Institute for Research in the Atmosphere, Colorado State University, Fort Collins, CO, USA. [7]Finnish Meteorological Institute, Earth Observation, Helsinki, Finland.
*Corresponding author. Email: annmarie.eldering@jpl.nasa.gov
†Present address: University of Toronto, Department of Physics, Toronto, Ontario, Canada.

use the transfer standard provided by a specially designed ground-based network of atmospheric observatories that comprise the Total Carbon Column Observing Network (TCCON) (*28*). Extensive comparisons have been made between OCO-2 satellite measurements coincident with the TCCON measurements (*29*, *30*). After correcting biases, the OCO-2 X_{CO_2} retrievals have median differences [for collections of >100 soundings] of less than 0.5 ppm and root-mean-square differences that are typically below 1.5 ppm (*30*). Simulation studies conducted before the launch of OCO estimated that large climate anomalies, like the 2003 European summer drought, which created a carbon anomaly of 0.5 gigatons C (*31*), would be detected by OCO, whereas scientific questions about smaller changes (on the order of 0.01 gigatons C) would not be addressed by OCO (*32*). The systematic biases from OCO-2 are consistent with the prelaunch design studies. As discussed in Chatterjee *et al.* (*33*), concentration changes of 0.5 ppm regionally can be detected with the OCO-2 measurements.

The interpretation of OCO-2 measurements is enhanced by measurements from the other Earth-observing satellites. The availability of measurements of trace gases such as nitrogen dioxide (NO_2) from the Ozone Monitoring Instrument (OMI), carbon monoxide (CO) from the Measurements of Pollution in the Troposphere (MOPITT) experiment, and many products from the Moderate Resolution Imaging Spectroradiometer (MODIS), have been used to disentangle the influence of complex and variable processes that contribute to the global carbon cycle (*34*–*37*).

Measuring plant fluorescence from space with OCO-2

Measurements of solar-induced chlorophyll fluorescence (SIF) from satellites offer insight into terrestrial gross primary productivity (GPP), the gross uptake of CO_2 through photosynthesis (*38*). The SIF signal, a small amount of light emitted during photosynthesis, is detected in remote sensing measurements of radiance within solar Fraunhofer lines. Retrieval methods were developed in recent years with the Japanese Greenhouse Gases Observing Satellite (GOSAT) Thermal and Near-Infrared Sensor for Carbon Observation–Fourier Transform Spectrometer (TANSO-FTS), Global Ozone Monitoring Experiment-2 (GOME-2) onboard MetOp-A, and OCO-2 measurements, and its potential for quantifying GPP is being assessed (*38*–*42*). Although the SIF signal is quite small—enhancements are typically less than 2% of the reflected sunlight (*43*)—the high signal-to-noise spectra from OCO-2 enable precise SIF measurements at high spatial resolution (*37*). Typically, the random component of the retrieval error varies between 0.3 and 0.5 $Wm^{-2}\ \mu m^{-1}\ sr^{-1}$ (15 to 25% of typical peak values of SIF) in the 757-nm fitting window (*44*), but the errors are substantially reduced by a factor of $1/\sqrt{n}$ if single retrievals (from individual soundings) are binned to gridded maps (n is the number of soundings per grid cell) at certain temporal averaging domains. In a companion paper in this issue, Sun *et al.* (*37*) describe OCO-2 SIF characteristics in detail and illustrate mechanistic connections between SIF and GPP. They show that when OCO-2 data are compared with GPP from flux tower measurements, well matched in spatial scale, they have correlation coefficients ranging from 0.89 to 0.99, with similar slopes for three different biomes. Earlier studies that used sparse data sets that had to be interpolated over time indicated biome-specific linear relationships.

Observing the carbon cycle from space with OCO-2

Maps of the X_{CO_2} data collected over three 32-day periods illustrate the most robust features of the carbon cycle (Fig. 2). The March/April 2015 distribution is characterized by enhanced X_{CO_2} in the Northern Hemisphere. During winter, uptake by plants is minimal while the breakdown or decay of plant material continues. As a result of this, together with the continual emissions from fossil fuel burning (e.g., elevated X_{CO_2} over China, Europe, and the southeast United States), X_{CO_2} reaches a seasonal maximum in the Northern Hemisphere during April just before temperatures increase enough to reawaken the biosphere from the low activity of winter. As illustrated in Fig. 3, active photosynthesis is manifest in the strong signal of plant fluorescence across the vegetated springtime Northern Hemisphere.

By June/July 2015, the distribution of X_{CO_2} and fluorescence observed by OCO-2 has changed dramatically compared with March/April (Fig. 2 for X_{CO_2}). Although fossil fuel emissions continue, the uptake of CO_2 by the terrestrial biosphere [e.g., figure 1 of (*37*)] has removed a large amount of CO_2 from the atmosphere over much of the Northern Hemisphere; the latitudinal gradient of X_{CO_2} has reversed. In 2015, OCO-2 observations indicate that the springtime drawdown began in Europe and propagated eastward across Asia and North America over the months of May and June. In some regions, X_{CO_2} declined by 7 ppm in only 1 month. Movie 1 illustrates the CO_2 from an atmospheric analysis, a product that merges OCO-2 observations with a high-resolution global model using a technique called data assimilation (*45*). The incorporation of OCO-2 observations corrects errors in the model's prediction of atmospheric CO_2 concentrations, and the model provides additional information about the vertical distribution of the gas and fills gaps in cloudy, data-sparse regions. Spanning March 2015 through the end of July 2015, the rapid reductions in CO_2 concentrations in the Northern Hemisphere during June are evident in movie 1, as are the complex pathways that transport CO_2 through the atmosphere, across oceans and continents.

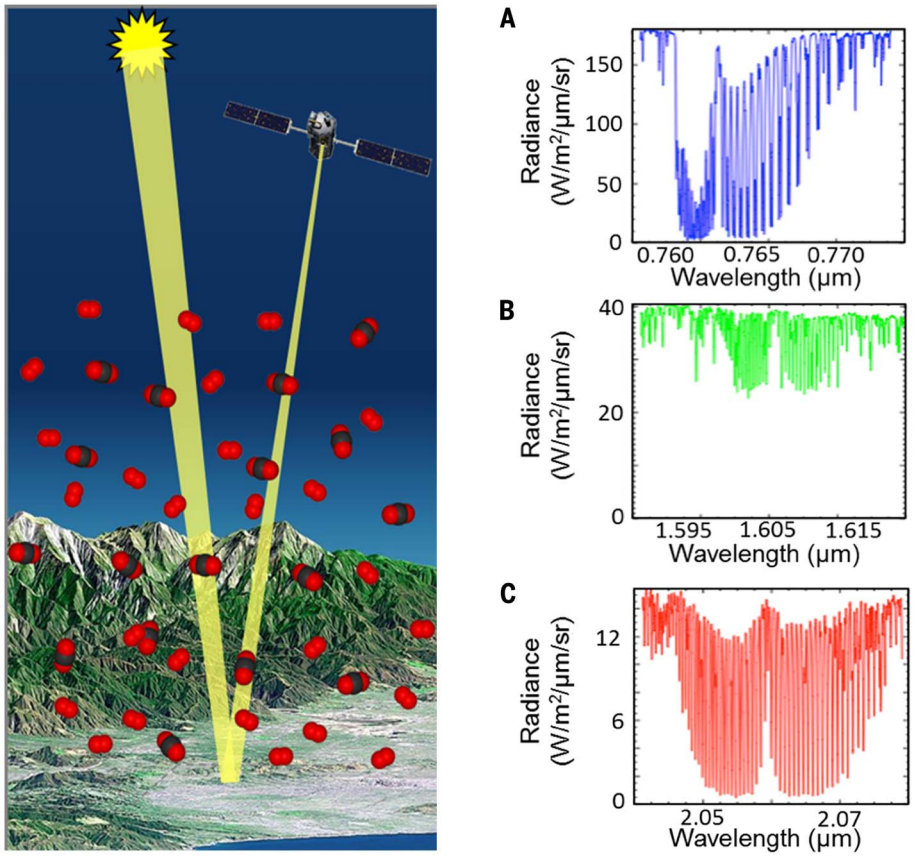

Fig. 1. OCO-2 detects sunlight that has traveled through the atmosphere and is reflected back to space. The sunlight is partially absorbed by the O_2 A-band (**A**) and the weak and strong CO_2 bands centered near 1.61 (**B**) and 2.06 μm (**C**).

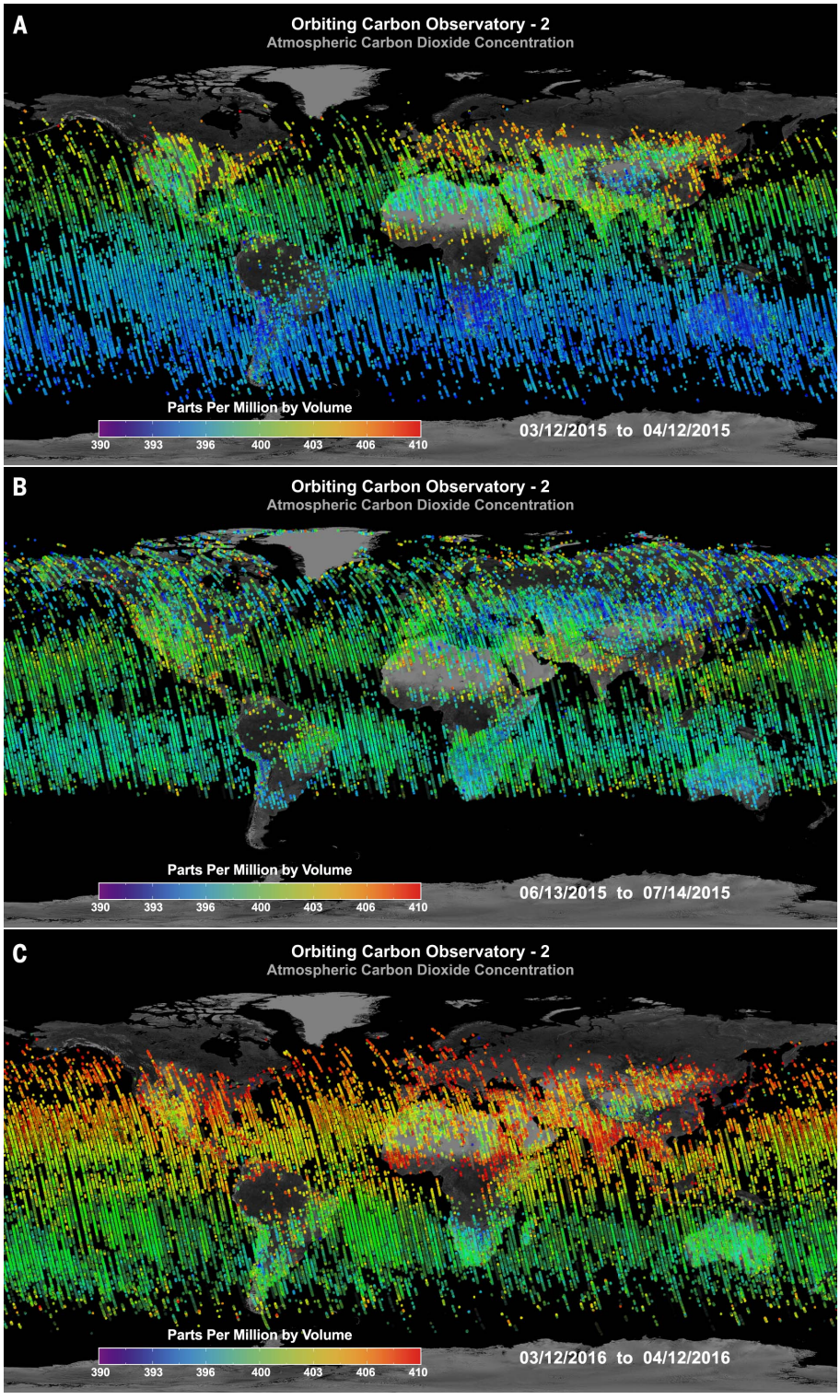

Fig. 2. Maps of OCO-2 X_{CO_2}. Maps of OCO-2 X_{CO_2} (bias corrected with quality flags applied) over 32-day periods in (**A**) March/April 2015, (**B**) June/July 2015, and (**C**) March/April 2016. The measurement area of each sounding has been exaggerated for visibility on a global scale.

By March/April 2016, the distribution of X_{CO_2} is similar to the year before, but with an increased concentration of ~3.5 ppm globally. A substantial fraction of this increase reflects emissions from fossil fuel burning. Direct evidence for these emissions includes the 1- to 3-ppm enhancements in X_{CO_2} over the regions with intense industrial activity. For example, Schwandner *et al.* (*46*) observe a local, persistent enhancement of 4 to 6 ppm in X_{CO_2} between OCO-2 measurements across the Los Angeles basin and the measurements that extend to the desert region to the north. The basin provides an ideal setting for such analyses, with a large urban population and accompanying emissions, and mountains to the north of the city, which trap air in the basin and provide a clear demarcation from the background region to the north. This is illustrated in Fig. 4 and in Schwandner *et al.* (*46*). More broadly, the spatial enhancements of X_{CO_2} due to the burning of fossil fuel across the Northern Hemisphere are illustrated in Fig. 5. Hakkarainen *et al.* (*34*) combined OCO-2 X_{CO_2} measurements with space-based observations of NO_2 from the OMI instrument, as well as the Open-Source Data Inventory for Anthropogenic CO_2 (ODIAC) emissions inventory (*47*). Using cluster analysis, they identified X_{CO_2} enhancements clearly linked to fossil fuel combustion, which are shown in Fig. 5.

Another large signal seen in the OCO-2 data is the effect of seasonal biomass burning in Africa on the X_{CO_2} concentrations (Fig. 6). CO_2 accounts for more than 90% of annual global fire carbon emissions in current emission inventories (*48*), and fire emissions are typically enhanced during El Niño periods. These emissions have typically been estimated from models rather than direct observations. Uncertainties in the extent of the burned area, the biomass density within the burned area, and the fraction of biomass emitted as CO_2, CO, and other species compromise the accuracy of the estimates (*49*–*51*). Top-down constraints on pyrogenic CO_2 could therefore provide a much-needed check on fire emissions estimates.

OCO-2 measurements were used to estimate the CO_2 emissions from Indonesian fires in 2015 (*35*). Indonesia experienced an exceptional number of fires in 2015 due to El Niño–related drought and slash-and-burn agricultural practices. Emissions databases such as the Global Fire Assimilation System (GFASv1.2) and the Global Fire Emission Database (GFEDv4s) estimated the CO_2 emission to be ~1100 megatons CO_2 between July and November 2015. Heymann *et al.* (*35*) analyzed OCO-2 X_{CO_2} observations collected over Indonesia during this period using two different modeling approaches. They estimate pyrogenic CO_2 emissions near 731 ± 271 megatons CO_2. This estimate is 37 and 31% lower than those in the GFASv1.2 and GFEDv4s emissions databases. Interestingly, the OCO-2 based estimates are consistent with pyrogenic CO_2 emissions estimates based on CO measurements from the MOPITT instrument on the Terra platform and fire radiative power estimates from Terra and Aqua MODIS (692 ± 213 megatons CO_2) (*52*). Hakkarainen (*34*) also clearly sees the enhanced X_{CO_2} from biomass burning in his anomaly analysis, although their results are aggregated over time, so the seasonality is not reported. The Northern Hemisphere African biomass emissions peak in January each year (*48*, *53*) and have a duration of 4 to 5 months. Figure 6 illustrates the growth phase of that cycle for 2 years of OCO-2 measurements.

Time series of the OCO-2 X_{CO_2} estimates clearly show the seasonal cycles and the latitudinal differences in those seasonal cycles that are similar

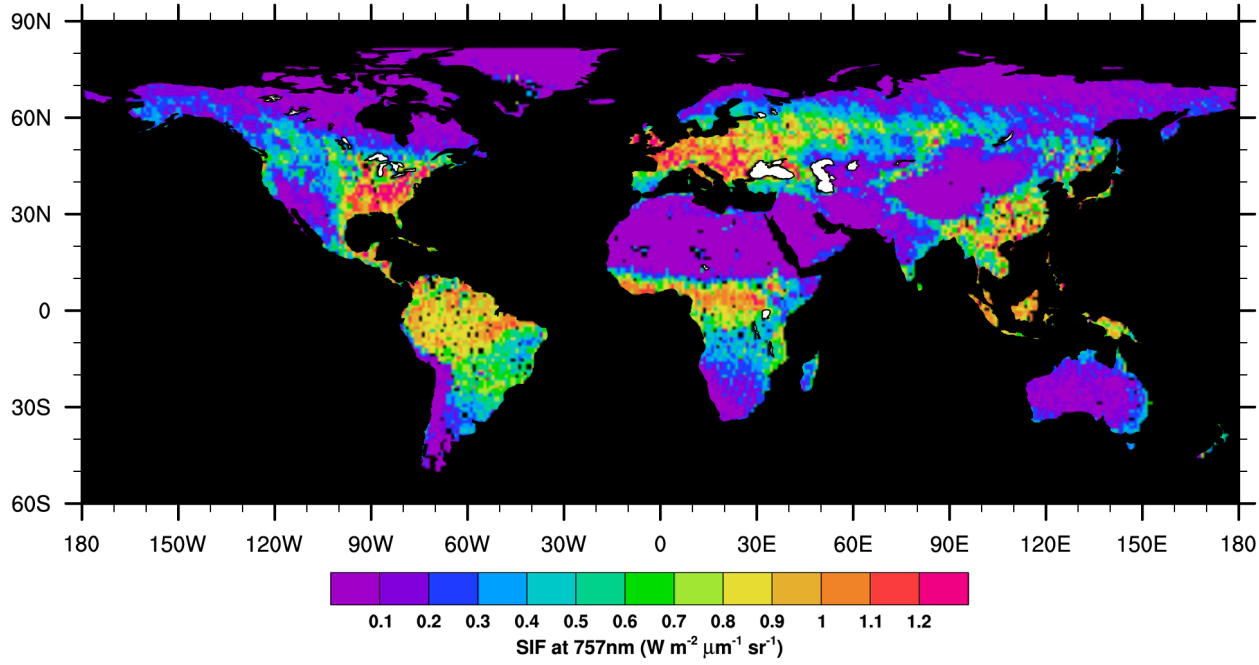

Fig. 3. The OCO-2 SIF retrieval at 757 nm on 1° by 1° grid for the spring (i.e., the mean of April-May-June for 2015 and 2016).

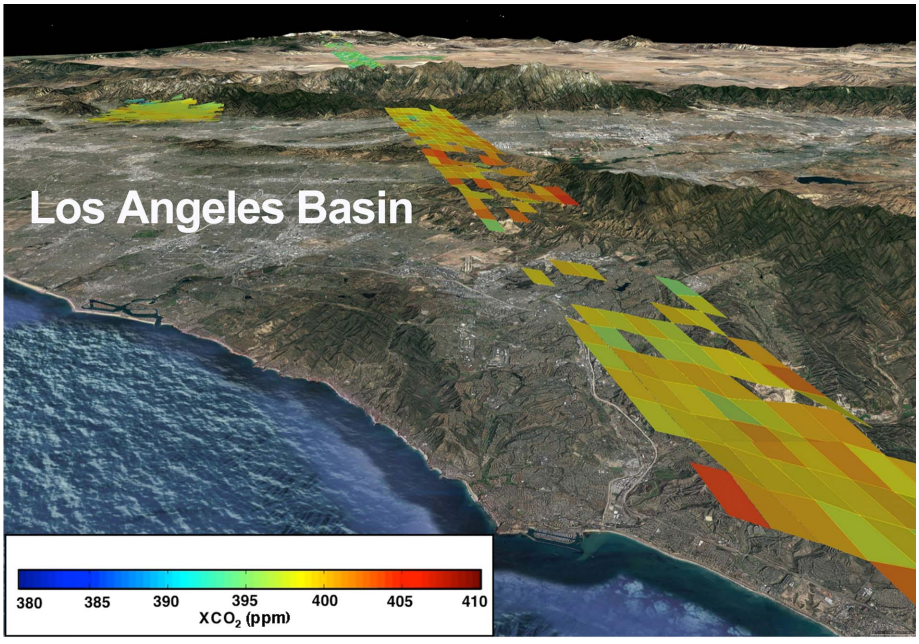

Fig. 4. OCO-2 X_{CO_2} measurements across the Los Angeles basin and into the desert north of Los Angeles taken during one overpass on 8 September 2015. The measurement swath is 10 km across. Two special sets of measurements taken for validation purposes—one at the California Institute of Technology and one at the Armstrong Flight Research Center—are also displayed.

to the record collected by ground-based networks. Figure 7 shows weekly average X_{CO_2} values for the South Pacific, the ocean around Hawaii, and a region over Europe and Asia. The South Pacific has a relatively flat seasonal cycle, because there are limited emissions and limited uptake by the terrestrial biosphere in this region. Around Hawaii, there is a stronger seasonal cycle, because it is influenced by the Northern Hemisphere springtime removal of CO_2 from the atmosphere by the terrestrial biosphere and the growth in atmospheric CO_2 in the winter, when human emissions are not balanced by natural removal mechanisms. Over Europe and Asia, there is a similar seasonal cycle, but the springtime X_{CO_2} reductions are more rapid, because these measurements are where the terrestrial biosphere is active.

The impact of the 2015–2016 El Niño on the carbon cycle

The massive 2015–2016 El Niño contributed to the anomalously large X_{CO_2} growth rate. The OCO-2 mission started approximately 6 months before the beginning of the El Niño. The 3 ppm global increase in X_{CO_2} recorded during this El Niño is one of the largest ever observed (*4*, *54*), consistent with previous research that has shown that global CO_2 increases anomalously during and in the year after large El Niños (*55*–*59*).

Diagnosis of the specific mechanisms responsible for the large CO_2 growth rates (e.g., the relative importance of changes in the ocean, the humid tropics, and the semiarid tropics), has been challenging due to a lack of observations of CO_2 in those regions (*60*). Data from the OCO-2 mission thus provides a window into the response of the ocean and land carbon cycle to this large-scale climate perturbation (*7*). Leveraging the broad coverage of OCO-2 data, Chatterjee *et al.* (*33*), Liu *et al.* (*36*), Heymann *et al.* (*35*), and Sun *et al.* (*37*) report on the quantification of CO_2 emissions sources and insights into the carbon cycle response to El Niño. These studies examine the role of ocean outgassing, drought, and fire as contributors to the increased growth rate of atmospheric CO_2.

Chatterjee *et al.* (*33*) used OCO-2 X_{CO_2} observations to study the temporal evolution of X_{CO_2} anomalies over the tropical Pacific Ocean. Using a combination of data from OCO-2, the TAO (Tropical Atmosphere Ocean) moored buoy array network (*61*) and MOPITT, they identify two

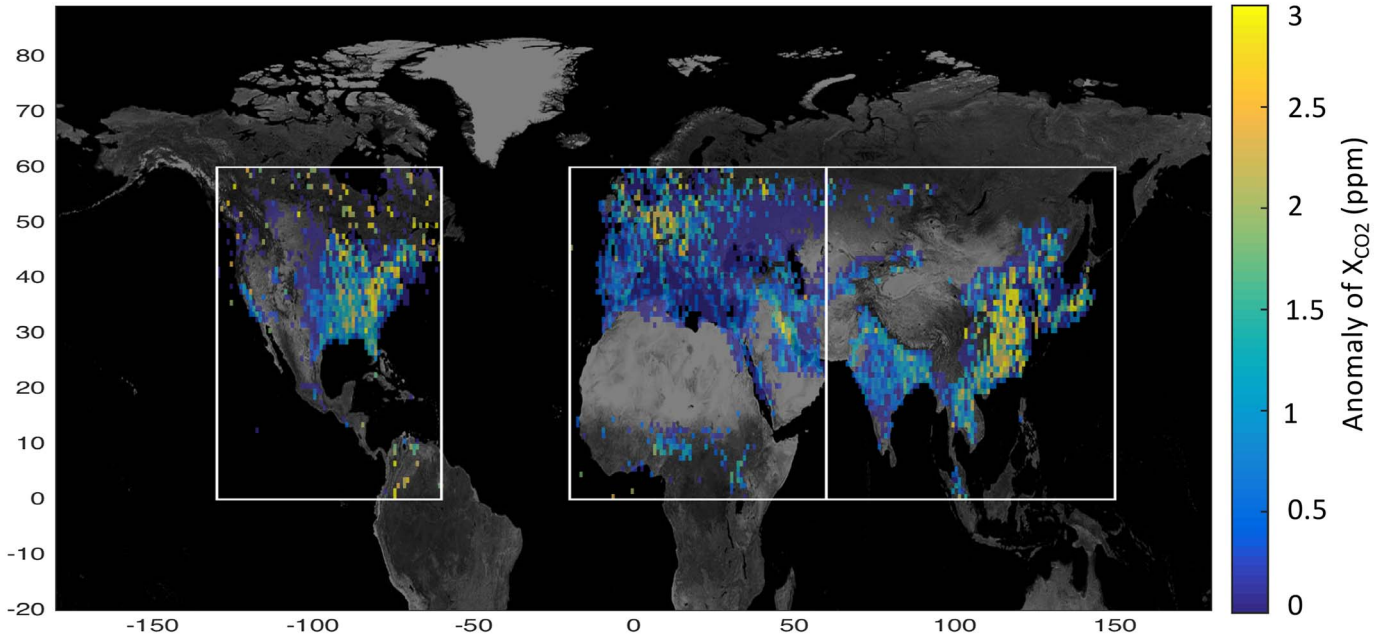

Fig. 5. Maps of the OCO-2 X_{CO_2} anomaly (mean in each grid box of the daily anomaly from the regional median) in 1° by 1° cells between September 2014 and April 2016. The anomalies are only plotted for the regions identified as clusters of enhancements due to fossil fuel burning in (*34*).

distinct phases in the response of atmospheric CO_2—an early response driven by reduction in CO_2 outgassing from the tropical Pacific Ocean followed by a lagged and much larger response driven by increased fluxes from the tropical land. To further elucidate the relationship between regional climate forcing and tropical biosphere carbon response, Liu *et al.* (*36*) contrast the 2015 carbon responses to 2011, which was a weak La Niña year with near-average temperature and precipitation over the tropical continents. They quantify net biosphere exchange (NBE) (i.e., the combined effects of respiration, fire, and GPP) for 2015 and 2011, respectively, by assimilating X_{CO_2} observations from OCO-2 and GOSAT into the NASA Carbon Monitoring System Flux (CMS-Flux) inversion system. To further partition the NBE into GPP, biomass burning, and residual respiration carbon fluxes, they optimized GPP and biomass burning fluxes with SIF from GOSAT (*62*) and CO observations from MOPITT (*63*), respectively.

The impacts of El Niño on the carbon cycle are complex (*33*, *36*): Temperature and rainfall changes in Southeast Asia, Africa, and South America are distinct, resulting in diverse carbon cycle impacts. X_{CO_2} decreased over the tropical Pacific Ocean, but flows of carbon were larger to the tropical atmosphere over all three continents. Over South America, dry conditions reduced GPP, resulting in a net increase in the flux of carbon to the atmosphere. Over Africa, higher atmospheric temperatures drove increased respiration (R_{eco}) but near normal GPP, increasing carbon flux to the atmosphere. Southeast Asia experienced higher temperatures and dry conditions, increased vulnerability to fire from land use, and increased emissions of CO_2. See Liu *et al.* (*36*) for additional discussion.

OCO-2 measurements in context of other remote sensing data

OCO-2 is not the first instrument to measure CO_2 from space, but its data have unique characteristics relative to existing data sets. Space-based measurements of CO_2 have been made in the thermal infrared beginning in the early 2000s with the Atmospheric Infrared Sounder (*64*) and are now being made by several other instruments. However, extracting surface source/sink information from these measurements has been largely unsuccessful, owing to their low sensitivity to near-surface CO_2, which provides the most information on surface exchange (*65*, *66*). The SCanning Imaging Absorption spectroMeter for Atmospheric CHartographY (SCIAMACHY) instrument made near-infrared measurements of column CO_2 from 2002 to 2012, although with relatively coarse spatial resolution (30 × 60 km^2) and lower sensitivity (4 to 8 ppm) (*67*–*70*). The Japanese GOSAT mission launched in 2009 (*71*, *72*) was the first mission whose primary goal was to measure greenhouse gases (carbon dioxide and methane) from space. The GOSAT mission has fostered considerable international scientific collaboration, leading to a deeper understanding of the utility of total column CO_2 measurements from space. The GOSAT CO_2 observations have formed the backbone of a number of important scientific studies. The primary limitation of the GOSAT measurement scheme is its low sounding density, with a single, 85-km^2 measurement per 250 km, resulting in fewer than 1000 cloud-free soundings each day.

The CO_2 seasonal cycle has also been studied with SCIAMACHY and GOSAT data (e.g., *73*, *74*–*76*). The GOSAT measurements have been used to characterize a number of relatively large disturbances to the carbon cycle, including reduced carbon uptake in 2010 due to the Eurasia heat wave (*77*), larger than average carbon fluxes in tropical Asia in 2010 due to above-average temperatures (*78*), and anomalous carbon uptake in Australia (*79*). Parazoo *et al.* (*62*) used GOSAT X_{CO_2} and SIF estimates to better understand the carbon balance of southern Amazonia. Ross *et al.* (*80*) used GOSAT data to obtain information on wildfire CH_4:CO_2 emission ratios. Buchwitz *et al.* (*67*) provide an excellent overview of the SCIAMACHY and GOSAT remote sensing data sets.

The OCO-2 measurements have a higher spatial resolution than GOSAT and SCIAMACHY and include a larger number of measurements per day. OCO-2 was designed as a sampling mission, not a mapping mission, so it only samples a small fraction of the globe each day. Although it would be desirable to have high-precision measurements over the whole globe daily, current limitations in remote sensing create a trade-off in sampling coverage and measurement precision (*81*), and OCO-2 has been designed to have sparse sampling and high precision (*18*, *82*). This trade-off allows OCO-2 to capture the data required for assessing regional fluxes of CO_2 across the globe (*32*, *82*). Additionally, OCO-2 X_{CO_2} high precision allows the detection of small changes in regional concentrations (*33*), including the observations, from a single overpass, of gradients across cities that the measurement path happens to cross (*46*).

Similarly, SIF has been derived from SCIAMACHY (*41*, *83*), GOME-2 (*84*) and GOSAT measurements

(39, 84) as well as OCO-2. Although these data sets span a longer period of time than OCO-2, the OCO-2 SIF product has a smaller footprint (<3 km^2 for OCO-2 versus 2400 km^2 for GOME-2, 1800 km^2 for SCIAMACHY, and 85 km^2 for GOSAT) and a higher signal-to-noise ratio (44, 85). As discussed in detail in Sun *et al.* (37), the OCO-2 SIF data provide higher single-sounding precision then the other data sets, with reduced spatial coverage of the globe. These characteristics are valuable for improving our mechanistic understanding, because the OCO-2 data spatial resolution is well matched to ground-based measurements and the scales of heterogeneity in many ecosystems.

Looking forward, NASA's current plan calls for continued development of the space-based CO_2 and SIF record with OCO-3, which will be deployed on the International Space Station (ISS) no earlier than the fall of 2018. Although the OCO-2 and OCO-3 instruments are very similar (the core spectrometer used by OCO-3 was the flight spare for OCO-2), differences in the OCO-2 and ISS orbits and observing capabilities will further enhance the value of simultaneous measurements from these two sensors. In particular, from its near-polar, sun-synchronous orbit, OCO-2 can sample most of the globe but can only measure X_{CO_2} and SIF at ~1:30 p.m. local time. In contrast, although the moderate inclination of the ISS orbit restricts OCO-3 coverage to ±51° latitude, the orbit precesses in time, enabling X_{CO_2} and SIF observations from dawn to dusk. Finally, although OCO-2 can collect targeted measurements over only one to two sites each day, OCO-3 will use its fast-pointing mechanism to acquire thousands of measurements over up to a hundred 70 km by 70 km targets each day. Combining the OCO-2 and OCO-3 data sets will therefore enable carbon cycle investigations that require uniform sampling of the globe, as well as sampling of the diurnal cycle or compact sources, such as megacities.

The combined OCO-2/OCO-3 climate data record will provide a valuable baseline for the Geostationary Carbon Cycle Observatory (GeoCARB) mission, which was recently selected by the NASA Earth Ventures Program (86). GeoCARB will be NASA's first greenhouse gas sensor in geostationary orbit. If all goes as planned, GeoCARB will be ready for launch no earlier than 2021. It will deployed at 85°W longitude, where it can produce continuous global maps of X_{CO_2}, X_{CH_4}, and X_{CO} over the North and South American continents. Internationally, a number of near-infrared CO_2 measurements are beginning or planned, including China's TanSat, which was launched in December 2016 (87, 88), the Japanese GOSAT-2, planned to launch in 2018 (89), and the French Space Agency's (Centre National d'Etudes Spatiales) MicroCARB, with a planned launch in 2020 (90).

The record of SIF measurements will also expand greatly in the future. Sensors that will return SIF measurement include OCO-3, TROPOspheric Monitoring Instrument (TROPOMI) (91), ESA FLEX (92), GOSAT-2, MicroCARB, and GeoCARB. As with CO_2, these new missions will both extend the SIF record in time and provide new capabilities, such as sampling over a range of daylight hours and with a range of spatial resolutions.

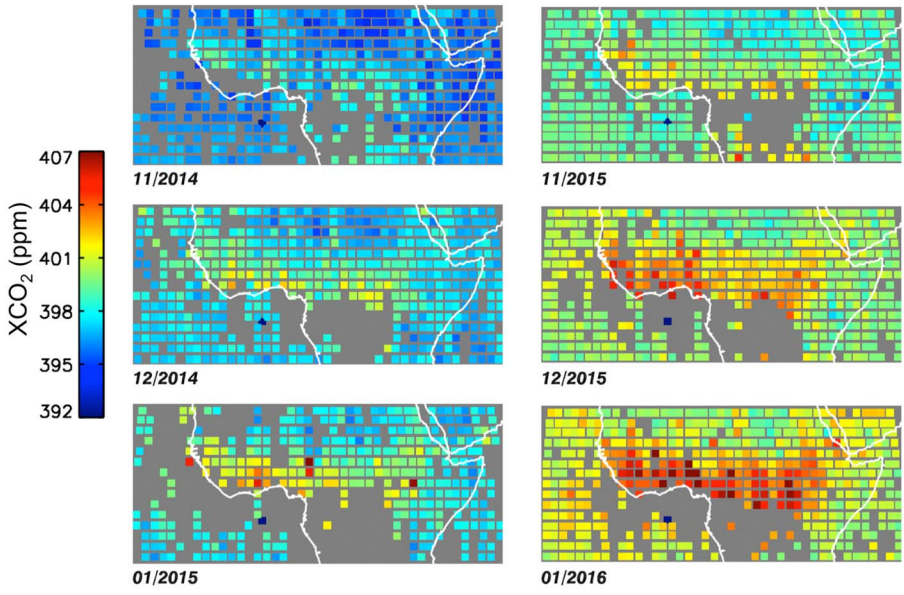

Fig. 6. Maps of OCO-2 X_{CO_2} over sub-Saharan Africa for the beginning of the biomass burning seasons of 2015 and 2016, showing the rapid regional increase in X_{CO_2}. The data have been averaged to 2° by 2° bins each month, after bias correction and quality screening were applied.

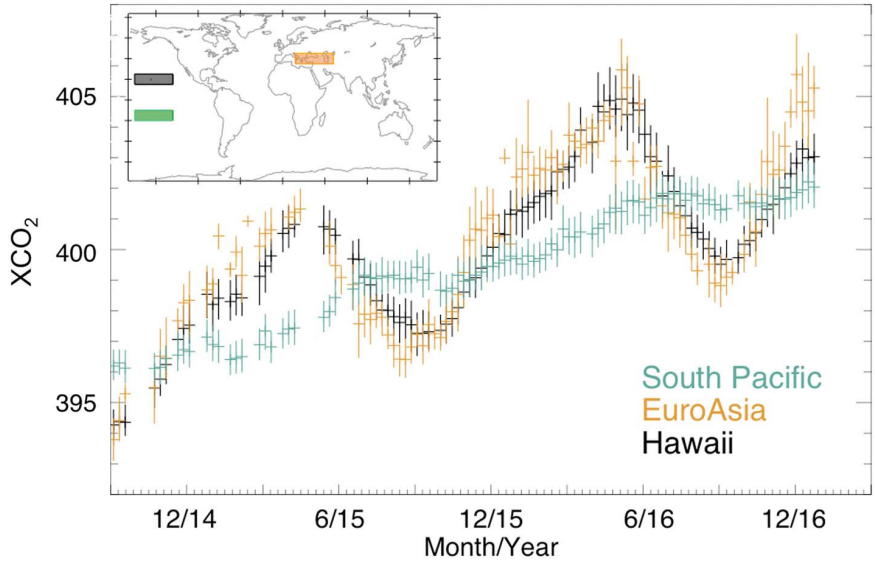

Fig. 7. Time series of weekly OCO-2 X_{CO_2} averages for regions around Hawaii, the Southern Pacific Ocean, and EuroAsia, showing the contrast of the seasonal cycle in the Northern and Southern Hemispheres that is clearly observed by OCO-2. The data have bias correction and quality screening applied.

Conclusions

The dense, global, X_{CO_2}, and SIF data sets from GOSAT and OCO-2 are being combined with data from MODIS, OMI, and MOPPIT and used to disentangle the processes driving the carbon cycle on regional scales. The accompanying reports in this collection use these data to discriminate the impacts of fossil fuel emissions, fires, and the 2015–2016 El Niño on the atmospheric CO_2 budget. A longer data record is needed to document the carbon cycle's response as the tropical climate relaxes back to its background state. An even longer record will be needed to fully characterize the interactions between the present-day carbon cycle and climate system. This information is crucial for the development and

validation of improved coupled carbon-climate models for predicting the carbon cycle's response to a warming climate. Fortunately, as OCO-2 completes its 2-year prime mission and begins its first extended mission, the spacecraft and instrument remain healthy, and data products with improved accuracy and coverage are in development.

REFERENCES AND NOTES

1. P. Ciais *et al.*, in *Climate Change 2013: The Physical Science Basis. Contribution of Working Group I to the Fifth Assessment Report of the Intergovernmental Panel on Climate Change* (Cambridge Univ. Press, 2014), pp. 465–570.
2. G. Marland, T. A. Boden, R. J. Andres, *Global, Regional, and National Fossil Fuel CO_2 Emissions. In Trends: A Compendium of Data on Global Change* (Carbon Dioxide Information Analysis Center, Oak Ridge National Laboratory, U.S. Department of Energy, Oak Ridge, TN, 2008).
3. C. Le Quéré *et al.*, Global carbon budget 2015. *Earth Syst. Sci. Data* **7**, 349–396 (2015). doi: 10.5194/essd-7-349-2015
4. M. R. Raupach *et al.*, The declining uptake rate of atmospheric CO_2 by land and ocean sinks. *Biogeosciences* **11**, 3453–3475 (2014). doi: 10.5194/bg-11-3453-2014
5. E. Dlugokencky, P. Tans, "Greenhouse Gas Reference Network Site Information" (Earth System Research Laboratory, Global Monitoring Division, 2017); https://www.esrl.noaa.gov/gmd/ccgg/ggrn.php.
6. C. L. Sabine *et al.*, The oceanic sink for anthropogenic CO_2. *Science* **305**, 367–371 (2004). doi: 10.1126/science.1097403; pmid: 15256665
7. D. Schimel, B. B. Stephens, J. B. Fisher, Effect of increasing CO_2 on the terrestrial carbon cycle. *Proc. Natl. Acad. Sci. U.S.A.* **112**, 436–441 (2015). doi: 10.1073/pnas.1407302112; pmid: 25548156
8. M. Reuter *et al.*, Satellite-inferred European carbon sink larger than expected. *Atmos. Chem. Phys.* **14**, 13739–13753 (2014). doi: 10.5194/acp-14-13739-2014
9. F. Chevallier *et al.*, Toward robust and consistent regional CO_2 flux estimates from in situ and spaceborne measurements of atmospheric CO_2. *Geophys. Res. Lett.* **41**, 1065–1070 (2014). doi: 10.1002/2013GL058772
10. J. Sarmiento *et al.*, Trends and regional distributions of land and ocean carbon sinks. *Biogeosciences* **7**, 2351–2367 (2010). doi: 10.5194/bg-7-2351-2010
11. D. S. Schimel, Terrestrial ecosystems and the carbon cycle. *Glob. Change Biol.* **1**, 77–91 (1995). doi: 10.1111/j.1365-2486.1995.tb00008.x
12. V. K. Arora *et al.*, Carbon–concentration and carbon–climate feedbacks in CMIP5 Earth system models. *J. Clim.* **26**, 5289–5314 (2013). doi: 10.1175/JCLI-D-12-00494.1
13. P. Friedlingstein *et al.*, Climate–carbon cycle feedback analysis: Results from the C4MIP model intercomparison. *J. Clim.* **19**, 3337–3353 (2006). doi: 10.1175/JCLI3800.1
14. E. Dlugokencky, P. Tans, "Trends in Atmospheric Carbon Dioxide" (Earth System Research Laboratory, Global Monitoring Division, 2017); https://www.esrl.noaa.gov/gmd/ccgg/trends/gr.html.
15. C. L. Zhao, P. P. Tans, Estimating uncertainty of the WMO mole fraction scale for carbon dioxide in air. *J. Geophys. Res. D Atmos.* **111**, D08S09 (2006). doi: 10.1029/2005JD006003
16. T. S. L'Ecuyer, J. H. Jiang, Touring the atmosphere aboard the A-Train. *Phys. Today* **63**, 36–41 (2010). doi: 10.1063/1.3463626
17. D. Crisp *et al.*, The orbiting carbon observatory (OCO) mission. *Adv. Space Res.* **34**, 700–709 (2004). doi: 10.1016/j.asr.2003.08.062
18. D. Crisp, C. E. Miller, P. L. DeCola, NASA Orbiting Carbon Observatory: Measuring the column averaged carbon dioxide mole fraction from space. *J. Appl. Remote Sens.* **2**, 023508–023514 (2008). doi: 10.1117/1.2898457
19. D. Crisp *et al.*, The on-orbit performance of the Orbiting Carbon Observatory-2 (OCO-2) instrument and its radiometrically calibrated products. *Atmos. Meas. Tech.* **10**, 59–81 (2017). doi: 10.5194/amt-10-59-2017
20. H. Bösch *et al.*, Space-based near-infrared CO_2 measurements: Testing the Orbiting Carbon Observatory retrieval algorithm and validation concept using SCIAMACHY observations over Park Falls, Wisconsin. *J. Geophys. Res. D Atmos.* **111**, D23302 (2006). doi: 10.1029/2006JD007080
21. C. O'Dell *et al.*, The ACOS CO_2 retrieval algorithm-Part 1: Description and validation against synthetic observations. *Atmos. Meas. Tech.* **5**, 99–121 (2012). doi: 10.5194/amt-5-99-2012
22. B. J. Connor *et al.*, Orbiting Carbon Observatory: Inverse method and prospective error analysis. *J. Geophys. Res. D Atmos.* **113**, D05305 (2008). doi: 10.1029/2006JD008336
23. H. Boesch, D. Baker, B. Connor, D. Crisp, C. Miller, Global characterization of CO_2 column retrievals from shortwave-infrared satellite observations of the Orbiting Carbon Observatory-2 mission. *Remote Sens.* **3**, 270–304 (2011). doi: 10.3390/rs3020270
24. A. Eldering *et al.*, The Orbiting Carbon Observatory-2: First 18 months of science data products. *Atmos. Meas. Tech.* **10**, 549–563 (2017). doi: 10.5194/amt-10-549-2017
25. T. E. Taylor *et al.*, Orbiting Carbon Observatory-2 (OCO-2) cloud screening algorithms: Validation against collocated MODIS Inf. Serv. and CALIOP data. *Atmos. Meas. Tech.* **9**, 973–989 (2016). doi: 10.5194/amt-9-973-2016
26. L. Mandrake *et al.*, "Lite Files, Warn Levels, and Bias Correction Determination, Version 1," *JPL Technical Report* (NASA Jet Propulsion Laboratory, California Institute of Technology, 2015).
27. D. Wunch *et al.*, A method for evaluating bias in global measurements of CO_2 total columns from space. *Atmos. Chem. Phys.* **11**, 12317–12337 (2011). doi: 10.5194/acp-11-12317-2011
28. D. Wunch *et al.*, The total carbon column observing network. *Philos. Trans. R. Soc. London Ser. A* **369**, 2087–2112 (2011). doi: 10.1098/rsta.2010.0240
29. D. Wunch *et al.*, *The Total Carbon Column Observing Network's GGG2014 Data Version* (Carbon Dioxide Information Analysis Center, Oak Ridge National Laboratory, Oak Ridge, TN, USA, 2015).
30. D. Wunch *et al.*, Comparisons of the Orbiting Carbon Observatory-2 (OCO-2) X_{CO2} measurements with TCCON. *Atmos. Meas. Tech.* **10**, 2209–2238 (2017). doi: 10.5194/amt-10-2209-2017
31. P. Ciais *et al.*, Europe-wide reduction in primary productivity caused by the heat and drought in 2003. *Nature* **437**, 529–533 (2005). doi: 10.1038/nature03972; pmid: 16177786
32. F. Chevallier, F. M. Bréon, P. J. Rayner, Contribution of the Orbiting Carbon Observatory to the estimation of CO_2 sources and sinks: Theoretical study in a variational data assimilation framework. *J. Geophys. Res. D Atmos.* **112**, D09307 (2007). doi: 10.1029/2006JD007375
33. A. Chatterjee *et al.*, Influence of El Niño on atmospheric CO_2 over the tropical Pacific Ocean: Findings from NASA's OCO-2 mission. *Science* **358**, eaam5776 (2017).
34. J. Hakkarainen, I. Ialongo, J. Tamminen, Direct space-based observations of anthropogenic CO_2 emission areas from OCO-2. *Geophys. Res. Lett.* **43**, 11400–11406 (2016). doi: 10.1002/2016GL070885
35. J. Heymann *et al.*, CO_2 emission of Indonesian fires in 2015 estimated from satellite-derived atmospheric CO_2 concentrations. *Geophys. Res. Lett.* **44**, 1537–1544 (2017). doi: 10.1002/2016GL072042
36. J. Liu *et al.*, Contrasting carbon cycle responses of the tropical continents to the 2015–2016 El Niño. *Science* **358**, eaam5690 (2017).
37. Y. Sun *et al.*, OCO-2 advances photosynthesis observation from space via solar-induced chlorophyll fluorescence. *Science* **358**, eaam5747 (2017).
38. C. Frankenberg, A. Butz, G. Toon, Disentangling chlorophyll fluorescence from atmospheric scattering effects in O_2 A-band spectra of reflected sun-light. *Geophys. Res. Lett.* **38**, L03801 (2011). doi: 10.1029/2010GL045896
39. C. Frankenberg *et al.*, New global observations of the terrestrial carbon cycle from GOSAT: Patterns of plant fluorescence with gross primary productivity. *Geophys. Res. Lett.* **38**, L17706 (2011). doi: 10.1029/2011GL048738
40. J. Joiner *et al.*, First observations of global and seasonal terrestrial chlorophyll fluorescence from space. *Biogeosciences* **8**, 637–651 (2011). doi: 10.5194/bg-8-637-2011
41. J. Joiner *et al.*, Filling-in of near-infrared solar lines by terrestrial fluorescence and other geophysical effects: Simulations and space-based observations from SCIAMACHY and GOSAT. *Atmos. Meas. Tech.* **5**, 809–829 (2012). doi: 10.5194/amt-5-809-2012
42. L. Guanter *et al.*, Retrieval and global assessment of terrestrial chlorophyll fluorescence from GOSAT space measurements. *Remote Sens. Environ.* **121**, 236–251 (2012). doi: 10.1016/j.rse.2012.02.006
43. C. Frankenberg, C. O'Dell, L. Guanter, J. McDuffie, Remote sensing of near-infrared chlorophyll fluorescence from space in scattering atmospheres: Implications for its retrieval and interferences with atmospheric CO_2 retrievals. *Atmos. Meas. Tech.* **5**, 2081–2094 (2012). doi: 10.5194/amt-5-2081-2012
44. C. Frankenberg *et al.*, Prospects for chlorophyll fluorescence remote sensing from the Orbiting Carbon Observatory-2. *Remote Sens. Environ.* **147**, 1–12 (2014). doi: 10.1016/j.rse.2014.02.007
45. L. E. Ott *et al.*, Assessing the magnitude of CO_2 flux uncertainty in atmospheric CO_2 records using products from NASA's Carbon Monitoring Flux Pilot Project. *J. Geophys. Res. D Atmos.* **120**, 734–765 (2015). doi: 10.1002/2014JD022411
46. F. M. Schwandner *et al.*, Spaceborne detection of localized carbon dioxide sources. *Science* **358**, eaam5782 (2017).
47. T. Oda, S. Maksyutov, A very high-resolution (1 km × 1 km) global fossil fuel CO_2 emission inventory derived using a point source database and satellite observations of nighttime lights. *Atmos. Chem. Phys.* **11**, 543–556 (2011). doi: 10.5194/acp-11-543-2011
48. G. R. van der Werf *et al.*, Global fire emissions and the contribution of deforestation, savanna, forest, agricultural, and peat fires (1997–2009). *Atmos. Chem. Phys.* **10**, 11707–11735 (2010). doi: 10.5194/acp-10-11707-2010
49. L. Giglio, J. T. Randerson, G. R. van der Werf, Analysis of daily, monthly, and annual burned area using the fourth-generation global fire emissions database (GFED4). *J. Geophys. Res. Biogeosci.* **118**, 317–328 (2013). doi: 10.1002/jgrg.20042
50. T. T. van Leeuwen *et al.*, Biomass burning fuel consumption rates: A field measurement database. *Biogeosciences* **11**, 7305–7329 (2014). doi: 10.5194/bg-11-7305-2014
51. S. Akagi *et al.*, Emission factors for open and domestic biomass burning for use in atmospheric models. *Atmos. Chem. Phys.* **11**, 4039–4072 (2011). doi: 10.5194/acp-11-4039-2011
52. V. Huijnen *et al.*, Fire carbon emissions over maritime southeast Asia in 2015 largest since 1997. *Sci. Rep.* **6**, 26886 (2016). doi: 10.1038/srep26886; pmid: 27241616
53. G. Roberts, M. Wooster, E. Lagoudakis, Annual and diurnal African biomass burning temporal dynamics. *Biogeosciences Discuss.* **5**, 3623–3663 (2008). doi: 10.5194/bgd-5-3623-2008
54. Q. Wang *et al.*, in *Remote Sensing of the Environment: 19th National Symposium on Remote Sensing of China* (International Society for Optics and Photonics, 2015), pp. 96690T-96690T-96696.
55. R. Bacastow, Modulation of atmospheric carbon dioxide by the Southern Oscillation. *Nature* **261**, 116–118 (1976). doi: 10.1038/261116a0
56. R. B. Bacastow *et al.*, Atmospheric carbon dioxide, the southern oscillation, and the weak 1975 El Niño. *Science* **210**, 66–68 (1980). doi: 10.1126/science.210.4465.66; pmid: 17751153
57. C. Keeling, R. Revelle, Effects of El Niño/Southern Oscillation on the atmospheric content of carbon dioxide. *Meteoritics* **20**, 437–450 (1985).
58. C. D. Keeling, T. P. Whorf, M. Wahlen, J. van der Plichtt, Interannual extremes in the rate of rise of atmospheric carbon dioxide since 1980. *Nature* **375**, 666–670 (1995). doi: 10.1038/375666a0
59. M. L. Thompson, I. Enting, G. Pearman, P. Hyson, Interannual variation of atmospheric CO_2 concentration. *J. Atmos. Chem.* **4**, 125–155 (1986). doi: 10.1007/BF00053775
60. J. L. Sarmiento, N. Gruber, in *Ocean Biogeochemical Dynamics* (Princeton Univ. Press, Princeton, New Jersey, 2006), pp. 392–453.
61. M. J. McPhaden, A. J. Busalacchi, D. L. Anderson, A TOGA retrospective. *Oceanography* **23**, 86–103 (2010). doi: 10.5670/oceanog.2010.26
62. N. C. Parazoo *et al.*, Terrestrial gross primary production inferred from satellite fluorescence and vegetation models. *Glob. Chang. Biol.* **20**, 3103–3121 (2014). doi: 10.1111/gcb.12652; pmid: 24909755
63. Z. Jiang *et al.*, Impact of model errors in convective transport on CO source estimates inferred from MOPITT CO retrievals. *J. Geophys. Res. D Atmos.* **118**, 2073–2083 (2013). doi: 10.1002/jgrd.50216
64. M. Chahine *et al.*, Satellite remote sounding of mid-tropospheric CO_2. *Geophys. Res. Lett.* **35**, L17807 (2008). doi: 10.1029/2008GL035022
65. F. Chevallier *et al.*, AIRS-based versus flask-based estimation of carbon surface fluxes. *J. Geophys. Res. D Atmos.* **114**, D20303 (2009). doi: 10.1029/2009JD012311
66. F.-M. Bréon, P. Ciais, Spaceborne remote sensing of greenhouse gas concentrations. *C. R. Geosci.* **342**, 412–424 (2010). doi: 10.1016/j.crte.2009.09.012

67. M. Buchwitz *et al*., Global satellite observations of column-averaged carbon dioxide and methane: The GHG-CCI XCO_2 and XCH_4 CRDP3 data set. *Remote Sens. Environ.* **2017**, 10.1016/j.rse.2016.12.027 (2017). doi: 10.1016/j.rse.2016.12.027
68. M. Reuter *et al*., Retrieval of atmospheric CO_2 with enhanced accuracy and precision from SCIAMACHY: Validation with FTS measurements and comparison with model results. *J. Geophys. Res. D Atmos.* **116**, D04301 (2011). doi: 10.1029/2010JD015047
69. M. Reuter *et al*., A method for improved SCIAMACHY CO_2 retrieval in the presence of optically thin clouds. *Atmos. Meas. Tech.* **3**, 209–232 (2010). doi: 10.5194/amt-3-209-2010
70. O. Schneising *et al*., Long-term analysis of carbon dioxide and methane column-averaged mole fractions retrieved from SCIAMACHY. *Atmos. Chem. Phys.* **11**, 2863–2880 (2011). doi: 10.5194/acp-11-2863-2011
71. A. Kuze, H. Suto, M. Nakajima, T. Hamazaki, Thermal and near infrared sensor for carbon observation Fourier-transform spectrometer on the Greenhouse Gases Observing Satellite for greenhouse gases monitoring. *Appl. Opt.* **48**, 6716–6733 (2009). doi: 10.1364/AO.48.006716; pmid: 20011012
72. T. Yokota *et al*., Global concentrations of CO_2 and CH_4 retrieved from GOSAT: First preliminary results. *Sci. Online Lett. Atmos.* **5**, 160–163 (2009). doi: 10.2151/sola.2009-041
73. M. Buchwitz *et al*., The Greenhouse Gas Climate Change Initiative (GHG-CCI): Comparison and quality assessment of near-surface-sensitive satellite-derived CO_2 and CH_4 global data sets. *Remote Sens. Environ.* **162**, 344–362 (2015). doi: 10.1016/j.rse.2013.04.024
74. M. Reuter *et al*., A joint effort to deliver satellite retrieved atmospheric CO_2 concentrations for surface flux inversions: The ensemble median algorithm EMMA. *Atmos. Chem. Phys.* **13**, 1771–1780 (2013). doi: 10.5194/acp-13-1771-2013
75. H. Lindqvist *et al*., Does GOSAT capture the true seasonal cycle of carbon dioxide? *Atmos. Chem. Phys.* **15**, 13023–13040 (2015). doi: 10.5194/acp-15-13023-2015
76. D. Wunch *et al*., The covariation of Northern Hemisphere summertime CO_2 with surface temperature in boreal regions. *Atmos. Chem. Phys.* **13**, 9447–9459 (2013). doi: 10.5194/acp-13-9447-2013
77. S. Guerlet *et al*., Reduced carbon uptake during the 2010 Northern Hemisphere summer from GOSAT. *Geophys. Res. Lett.* **40**, 2378–2383 (2013). doi: 10.1002/grl.50402
78. S. Basu *et al*., The seasonal variation of the CO_2 flux over Tropical Asia estimated from GOSAT, CONTRAIL, and IASI. *Geophys. Res. Lett.* **41**, 1809–1815 (2014). doi: 10.1002/2013GL059105
79. R. Detmers *et al*., Anomalous carbon uptake in Australia as seen by GOSAT. *Geophys. Res. Lett.* **42**, 8177–8184 (2015). doi: 10.1002/2015GL065161
80. A. N. Ross, M. J. Wooster, H. Bösch, R. Parker, First satellite measurements of carbon dioxide and methane emission ratios in wildfire plumes. *Geophys. Res. Lett.* **40**, 4098–4102 (2013). doi: 10.1002/grl.50733
81. W. J. Larson, J. R. Wertz, "Space mission analysis and design" (Microcosm, Inc., Torrance, CA, 1992).
82. C. Miller *et al*., Precision requirements for space-based data. *J. Geophys. Res. D Atmos.* **112**, D10314 (2007). doi: 10.1029/2006JD007659
83. J. Joiner, Y. Yoshida, L. Guanter, E. M. Middleton, New methods for the retrieval of chlorophyll red fluorescence from hyperspectral satellite instruments: Simulations and application to GOME-2 and SCIAMACHY. *Atmos. Meas. Tech. Discuss.* **9**, 3939–3967 (2016). doi: 10.5194/amt-9-3939-2016
84. J. Joiner *et al*., The seasonal cycle of satellite chlorophyll fluorescence observations and its relationship to vegetation phenology and ecosystem atmosphere carbon exchange. *Remote Sens. Environ.* **152**, 375–391 (2014). doi: 10.1016/j.rse.2014.06.022
85. C. Frankenberg *et al*., The Orbiting Carbon Observatory (OCO-2): Spectrometer performance evaluation using pre-launch direct sun measurements. *Atmos. Meas. Tech.* **8**, 301–313 (2015). doi: 10.5194/amt-8-301-2015
86. J. J. B. Kumer *et al*., in *SPIE Optical Engineering+ Applications* (International Society for Optics and Photonics, 2013), pp. 88670K-88670K-88616.
87. Y. Liu *et al*., in *AGU Fall Meeting Abstracts* (2012), vol. 1, pp. 01.
88. D. Liu *et al*., The retrieval algorithm for a satellite-borne CO_2-sounder: Preliminary results in near infrared band. *Optik-International Journal for Light and Electron Optics* **127**, 8613–8620 (2016). doi: 10.1016/j.ijleo.2016.06.072
89. M. Nakajima, A. Kuze, H. Suto, in *SPIE 8533, Sensors, Systems, and Next-Generation Satellites XVI* (International Society for Optics and Photonics, 2012), pp. 853306–853310.
90. C. Buil *et al*., in *SPIE Remote Sensing* (International Society for Optics and Photonics, 2011), pp. 817621-817621-817611.
91. L. Guanter *et al*., Potential of the TROPOspheric Monitoring Instrument (TROPOMI) onboard the Sentinel-5 Precursor for the monitoring of terrestrial chlorophyll fluorescence. *Atmos. Meas. Tech.* **8**, 1337–1352 (2015). doi: 10.5194/amt-8-1337-2015
92. S. Cogliati *et al*., Retrieval of sun-induced fluorescence using advanced spectral fitting methods. *Remote Sens. Environ.* **169**, 344–357 (2015). doi: 10.1016/j.rse.2015.08.022

ACKNOWLEDGMENTS

Retrieved Level 2 OCO-2 X_{CO_2} (version v7Br) data used in this study are archived in a permanent repository at NASA's Goddard Space Flight Center's Earth Sciences Data and Information Services Center (GES-DISC) and are also available at NASA's Jet Propulsion Laboratory (http://co2.jpl.nasa.gov). Part of the research described in this paper was carried out at the Jet Propulsion Laboratory, California Institute of Technology, under a contract with the National Aeronautics and Space Administration. The movie was created by B. Weir, L. Ott, S. Pawson, H. Mitchell, and G. Shirah at Goddard Space Flight Center and the Scientific Visualization Studio. B.W., L.O., and S.P. were supported by the NASA Carbon Monitoring System and the OCO-2 Science Team NASA Research Opportunities in Space and Earth Sciences (ROSES) projects. K. Yuen assisted with figure production. J.H. and J.T. were supported by the Academy of Finland Inversion Algorithms and Quantification of Uncertainties in Atmospheric Remote Sensing (INQUIRE) (grant number 267442) and Carbon Balance under Changing Processes if Arctic and Subarctic Cryosphere (CARB-ARC) (grant number 285630) projects.

SUPPLEMENTARY MATERIALS

www.sciencemag.org/content/358/6360/eaam5745/suppl/DC1
Movie S1

11 December 2016; accepted 12 July 2017
10.1126/science.aam5745

The Orbiting Carbon Observatory-2 early science investigations of regional carbon dioxide fluxes

A. Eldering, P. O. Wennberg, D. Crisp, D. S. Schimel, M. R. Gunson, A. Chatterjee, J. Liu, F. M. Schwandner, Y. Sun, C. W. O'Dell, C. Frankenberg, T. Taylor, B. Fisher, G. B. Osterman, D. Wunch, J. Hakkarainen, J. Tamminen and B. Weir

Science **358** (6360), eaam5745.
DOI: 10.1126/science.aam5745